A simple grand canonical approach to compute the vapor pressure of bulk and finite size systems

Matías H. Factorovich, Valeria Molinero, and Damián A. Scherlis

Citation: The Journal of Chemical Physics **140**, 064111 (2014); doi: 10.1063/1.4865137
View online: http://dx.doi.org/10.1063/1.4865137
View Table of Contents: http://scitation.aip.org/content/aip/journal/jcp/140/6?ver=pdfcov
Published by the AIP Publishing

A simple grand canonical approach to compute the vapor pressure of bulk and finite size systems

Matías H. Factorovich,[1] Valeria Molinero,[2] and Damián A. Scherlis[1]
[1]*Departamento de Química Inorgánica, Analítica y Química Física/INQUIMAE, Facultad de Ciencias Exactas y Naturales, Universidad de Buenos Aires, Ciudad Universitaria, Pab. II, Buenos Aires C1428EHA, Argentina*
[2]*Department of Chemistry, University of Utah, 315 South 1400 East, Salt Lake City, Utah 84112-0850, USA*

(Received 4 November 2013; accepted 28 January 2014; published online 13 February 2014)

In this article we introduce a simple grand canonical screening (GCS) approach to accurately compute vapor pressures from molecular dynamics or Monte Carlo simulations. This procedure entails a screening of chemical potentials using a conventional grand canonical scheme, and therefore it is straightforward to implement for any kind of interface. The scheme is validated against data obtained from Gibbs ensemble simulations for water and argon. Then, it is applied to obtain the vapor pressure of the coarse-grained mW water model, and it is shown that the computed value is in excellent accord with the one formally deduced using statistical thermodynamics arguments. Finally, this methodology is used to calculate the vapor pressure of a water nanodroplet of 94 molecules. Interestingly, the result is in perfect agreement with the one predicted by the Kelvin equation for a homogeneous droplet of that size. © *2014 AIP Publishing LLC*. [http://dx.doi.org/10.1063/1.4865137]

I. INTRODUCTION

The characterization of the gas-liquid equilibrium of a fluid, including the estimation of the vapor pressure as a function of temperature, pressure, composition, or interfacial curvature, is of extreme relevance from a general chemical-physics perspective, but also in countless applications related to adsorption,[1] materials engineering,[2–6] catalysis,[7–9] and environmental and atmospheric chemistry.[10–12] A number of methods exists to access computationally the point of coexistence and the vapor pressure of a liquid. The Gibbs ensemble Monte Carlo approach by Panagiotopoulos, based on particle exchange between two reservoirs containing the two phases in equilibrium, is possibly the most widespread.[13–15] Grounded on a different conception, the path-sampling techniques explore the configurations or contiguous macrostates connecting the two phases of interest, integrating the free-energy along the path. Examples implementing this strategy include various schemes like the expanded ensemble,[16] simulated tempering,[17] or adaptive umbrella sampling.[18] A review on these family of techniques can be found in Ref. 19. The more recent transition matrix Monte Carlo method (TMMC) originally applied to low-dimensional model systems,[20–24] is an efficient variation of these approaches which has been proved accurate and versatile to identify states in coexistence.[25,26] Errington has recently published a series of papers summarizing many of these contributions to the calculation of interfacial and coexistence phenomena in different molecular systems.[27–29]

However, most of these methods cannot be adapted in a simple way to capture the vapor pressure of an interface of arbitrary shape or size. In particular, the vapor pressure of nanodroplets or molecular aggregates is very difficult to access experimentally, though it is of a fundamental interest in areas like classical nucleation theory.[12] In some occasions, estimates have been obtained for Lennard-Jones models employing molecular dynamics simulations with constant number of particles.[30–34] The vapor pressures of nanoaggregates computed using this route, though, exhibit large uncertainties, due to the small number of particles in the vapor phase and to the infrequent collisions in the vapor.[31,32]

In this article, we propose a simple approach based on grand canonical simulations to accurately calculate the vapor pressure of bulk and finite interfaces. Indeed, this method (which will be referred to as GCS, from grand canonical screening) just requires to span a range of different chemical potentials using a conventional grand canonical scheme, and therefore it is straightforward to implement for any kind of interface. In the first place, we compare the results of our procedure with those obtained from the Gibbs ensemble method for the cases of the SPC/E water and argon potentials. Next, we apply it to obtain the vapor pressure of the coarse-grained mW water model, to show that the computed value of P_0 is in excellent agreement with the one formally predicted using statistical thermodynamics arguments. Then, we present an analysis of the precision and the magnitude of the errors associated with the GCS methodology. Finally, we employ it to calculate the vapor pressure of a water droplet of 94 molecules, with a diameter of about 1.7 nm, showing that the result is in agreement with the Kelvin equation if the Tolman correction is considered.

II. METHODOLOGY

In this study, both molecular dynamics and Monte Carlo simulations were performed in the grand canonical ensemble. We will refer to these two techniques by GCMD and GCMC, respectively. In particular, GCMD calculations were carried out using the program LAMMPS,[35] which, properly modified, allows for grand canonical simulations with monoatomic models with a high computational efficiency. Since grand canonical simulations within the LAMMPS package are

only feasible for monoatomic potentials, we also employed the public software Towhee for Monte Carlo molecular modelling,[36] which was applied to the atomistic SPC/E water model.[37]

Grand canonical molecular dynamics schemes introduce Metropolis Monte Carlo sampling throughout the dynamical evolution to allow for particle exchange with a reservoir, hence preserving a temporal description at a controlled chemical potential. The algorithm reproduces a grand-canonical ensemble where particles can be displaced, deleted or created in the simulation box. In the present implementation the movement of the particles is ruled by the integration of the Newton equations using the Verlet algorithm at constant temperature, which is controlled with the Nosé-Hoover thermostat. Insertion and deletion attempts are effected on single particles with equal probability anywhere in the box, adopting the usual acceptance criteria of the Monte Carlo grand-canonical algorithm.[15,38] The vapor may be treated as an ideal gas or as a real gas introducing fugacity coefficients. Along the grand canonical dynamics, a number of attempts for particle insertion and deletion are carried at every time-step: this number is the so called GC/MD ratio. It is desirable to keep this parameter as low as possible to minimize computer time, but in turn it must be high enough to ensure that the target chemical potential is reached during the simulation.[39,40] GC/MD ratios in the range 20–100 have been typically used in previous studies.[39–41] In our simulations a GC/MD ratio of 20 was adopted, which is common in the literature and gives converged results for the systems examined here.

An analogous scheme was employed in the grand canonical Monte Carlo simulations, for which the displacement, rotation, removal or insertion of a molecule were all equally probable. The magnitudes of molecular displacements and rotations were adjusted on the fly to fit a 50% acceptance ratio. In grand canonical simulations performed with the Towhee code, the pressure is not readily accessible: the acceptance criterion for insertion and deletion is based on the chemical potential, without a direct connection to P. The relation between μ and P, given by $\mu = \mu^{\theta} + k_B T \ln(P\phi/k_B T)$, with ϕ the fugacity coefficient, is not useful since we ignore the reference chemical potential μ^{θ} for the SPC/E model. Then, a possible way to estimate the pressure corresponding to a GCMC calculation with this code, is to run a single Monte Carlo simulation in the isothermal-isobaric (NPT) ensemble at a fixed pressure P^{NPT}, where the chemical potential μ^{NPT} can be computed, e.g., with the Widom insertion method. If ϕ is the fugacity coefficient, for each of these ensembles holds

$$\mu^{NPT} = \mu^0(T) + k_B T \ln\left(P^{NPT}\phi(P^{NPT})/k_B T\right),$$

$$\mu^{GCMC} = \mu^0(T) + k_B T \ln\left(P^{GCMC}\phi(P^{GCMC})/k_B T\right),$$

where the connection is attained by subtracting both equations:

$$P^{GCMC} = \frac{\phi(P^{NPT})}{\phi(P^{GCMC})} P^{NPT} e^{\left(\frac{\mu^{GCMC}-\mu^{NPT}}{k_B T}\right)}. \quad (1)$$

If the ideal gas approximation is valid, or if P^{GCMC} and P^{NPT} are very close, the ratio between the fugacity coefficients can be taken to be 1.

In the present study argon and water were modelled, using a Lennard-Jones potential with a cutoff of 7σ in the former case,[42] and both the SPC/E[37] and the mW[43] models for H_2O. The mW model represents each molecule as a single particle interacting through anisotropic short-ranged potentials that encourage "hydrogen-bonded" water structures. It adopts the short-ranged interaction form of the Stillinger-Weber force-field, which consists of a sum of two-body attraction terms favoring high coordination, and three-body repulsion terms reinforcing tetrahedral hydrogen-bonded configurations.[43] In recent years, the mW model has repeatedly been applied to explain the behavior of water in various conditions and regimes (see, for example, Ref. 44, and references therein). Periodic boundary conditions were used in all axes, setting the dimensions of the simulation box as to avoid interactions between images.

III. RESULTS AND DISCUSSION

A. Computation of the vapor pressure: Description of the GCS approach and application to argon and SPC/E water

To obtain the vapor pressure, various grand canonical simulations in the presence of an interface, must be conducted successively at different chemical potentials around the presumed equilibrium value. The procedure described here is equally valid for either GCMC or GCMD simulations. As each one of these simulation evolves, the total number of molecules N may rise or drop, depending on whether the magnitude of the chemical potential μ is, respectively, above or below the equilibrium value. Hence, μ_{eq} can be identified by spanning μ to find the condition for which N remains constant, or, more practically, for which the average derivative of N with respect to the simulation step changes from negative to positive. The precision in the characterization of the equilibrium point may be increased by narrowing down the chemical potential window.

In the case of a droplet, when the value of μ fixed in the simulation is above the value of μ_{eq} corresponding to the initial curvature of the interface, condensation occurs leading to an increase in radius, which in turn diminishes the magnitude of μ_{eq}. In this way the growth of the droplet continues until the simulation box is completely filled. Conversely, if μ is below μ_{eq} at the beginning of the simulation, the evaporation proceeds until all particles have disappeared. One possible way to understand this is by looking at the change of the free energy as a function of nanodroplet radius, described by the Kelvin equation in the context of classical nucleation theory and illustrated in Figure 1.[12] Each curve in the figure corresponds to a different value of the chemical potential μ, which is fixed in a grand canonical simulation (or in an experiment at constant pressure) and therefore the evolution of the system is constrained to only one of the curves. In our procedure, we run independent simulations at different chemical potentials. If the initial radius of the droplet is r^* and μ is lower than the equilibrium value (blue curve), the minimization of the free energy would lead to the evaporation of the cluster. For the same initial radius r^* but with μ larger than

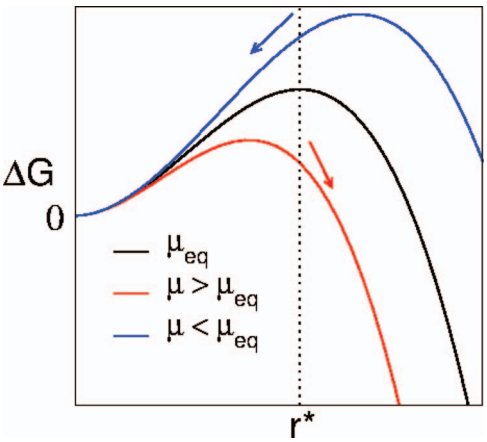

FIG. 1. Change of the Gibbs free energy (ΔG) involved in the formation of a droplet of radius r at different chemical potentials μ. A droplet of radius r^* is metastable at a chemical potential μ_{eq}. At a higher μ a droplet of this size will condense, whereas at a lower μ it will evaporate.

μ_{eq} (red curve), condensation would occur. By repeating this computational experiment for a given r^* at different chemical potentials, an upper and a lower bound can be found for μ_{eq}, with as much precision as desired at the expense of simulation time (see Sec. III C).

This procedure was applied to compute the bulk vapor pressure of the SPC/E water model at 300 K. At this temperature, the vapor in equilibrium may be assumed to be ideal: this is a common choice in grand canonical simulations of H_2O near ambient conditions.[45–48] The determination of the equilibrium point was accomplished through a series of GCMC simulations of a water slab initially consisting of 240 molecules and exposing two planar interfaces to the vacuum, contained in a box of $1.5 \times 1.5 \times 55.5$ nm^3 in periodic boundary conditions. Figure 2 depicts the number of molecules as a function of time for several choices of μ, which can be related to the pressure via Eq. (1). The system slips from evaporation to condensation when the pressure jumps from 7.4 mbar to 8.8 mbar: this allows to situate the equilibrium vapor pressure at 8.1 ± 0.7 mbar (this uncertainty could be reduced by further exploration inside the 7.4–8.8 mbar range). This outcome is in excellent agreement with the value of 7.65 ± 0.38 mbar reported for SPC/E water at 300 K by Liu and Monson on the basis of simulations in the Gibbs ensemble.[49] Less recent calculations also based on the Gibbs ensemble methodology by Errington and Panagiotopoulos estimated a value of 10 mbar.[50] It must be noted that these results are less than one third of the experimental vapor pressure; this inaccuracy is common to other atomistic models of water such as TIP4P.[51,52]

As a final validation, we have explored the vapor pressure of liquid argon at different temperatures. To this end we performed a set of GCMD runs with the program LAMMPS, modelling the liquid argon phase with 4096 molecules in a box of dimensions $4.8 \times 4.8 \times 30$ nm^3. The states of the gas phase on the coexistence curve cannot be assumed ideal above 90 K, so the Ar pressures were corrected using the fugacity coefficients. The procedure to correct the pressure and the fugacity coefficients for this system are reported in the Appendix. In Figure 3 the results obtained using our approach are compared with experiments and with data from Gibbs ensemble calculations from different groups.[13,53] Our results show very good agreement with the values reported by Panagiotopoulos *et al.*[13]

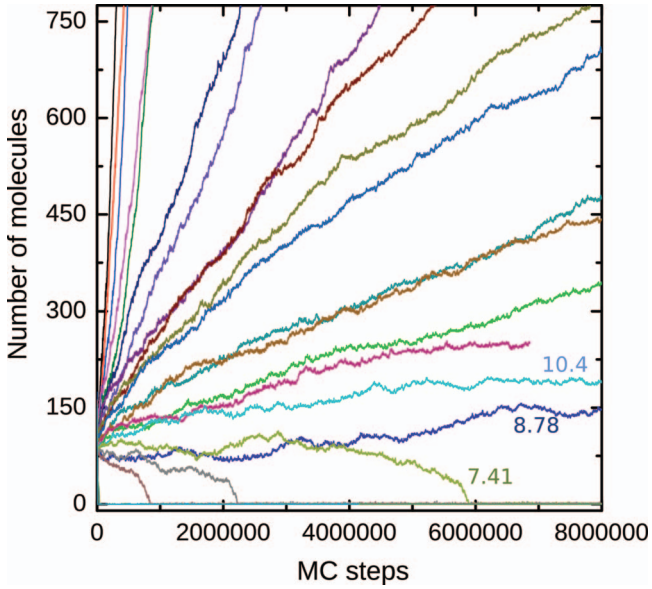

FIG. 2. Number of water molecules versus GCMC simulation step of a planar vapor-liquid interface using the SPC/E model. Each curve corresponds to a different pressure, which is indicated in mbar for those cases close to the equilibrium condition. For pressures lower than or equal to 7.41 mbar the number of molecules eventually decays to zero, while for pressures higher than or equal to 8.78 mbar the liquid phase grows and occupies the full simulation box.

B. The vapor pressure of the mW water model

The bulk vapor pressure of the mW model was calculated considering a water slab initially consisting of 4096 molecules and exposing two planar interfaces to the vacuum, contained in a box of $4.9 \times 4.9 \times 8.6$ nm^3 in periodic

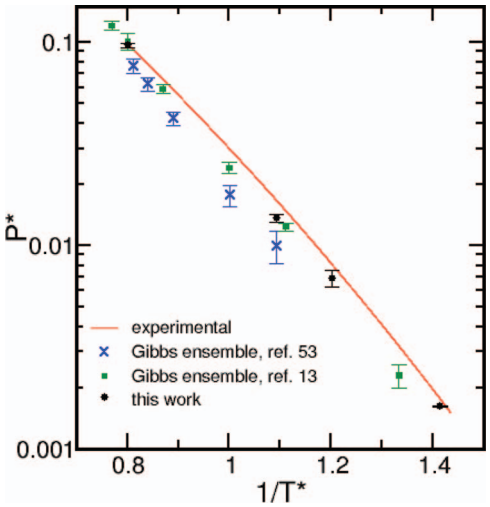

FIG. 3. Vapor pressure of bulk argon as a function of the inverse temperature (in reduced units). Data from Gibbs ensemble simulations were taken from Panagiotopoulos[13] and from Al-Matar.[53] The experimental curve shows the fitting by Drii and Rabinovich.[61]

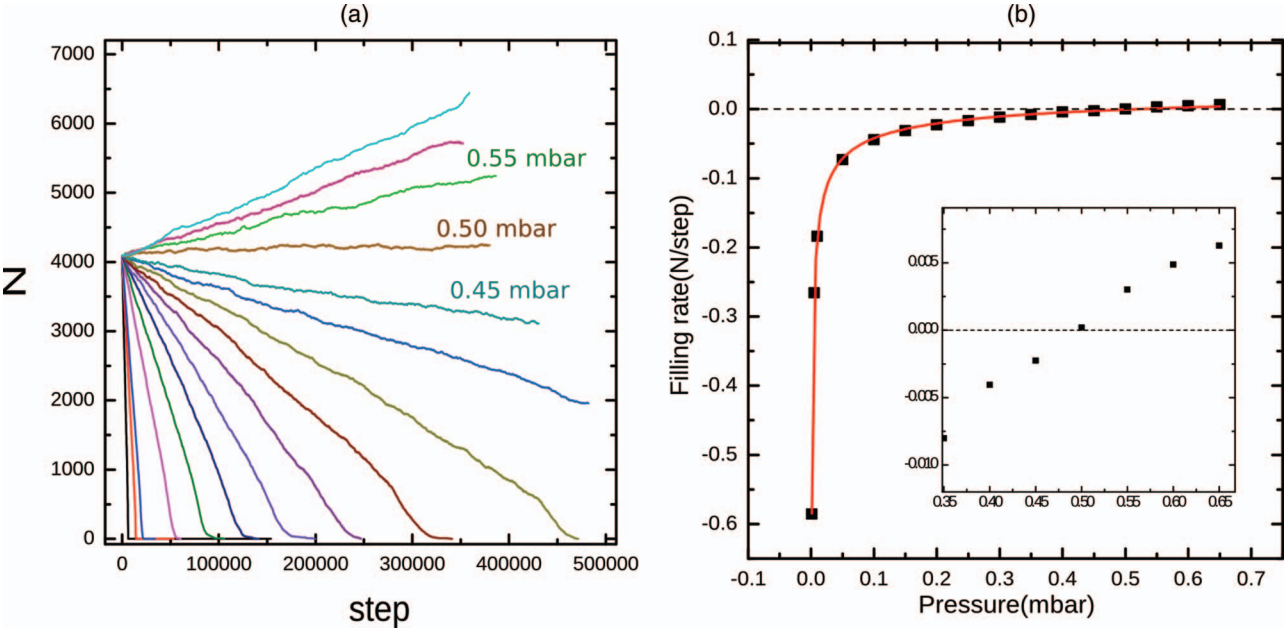

FIG. 4. (a) Evolution of the number of particles (N) as a function of time, in GCMD simulations of a planar vapor-liquid water interface represented with the mW model at different chemical potentials. The time step is 5 fs. The value of μ was varied to screen a range of pressures from 0.001 mbar (black line) to 0.6 mbar (cyan). (b) Rate of filling versus pressure. The two phases are in thermodynamical equilibrium when $dN/dt = 0$, for a pressure of 0.5 mbar. The inset zooms in on the zero intercept region.

boundary conditions. Figure 4(a) shows the number of molecules as a function of time resulting from GCMD simulations at different values of μ. To identify the equilibrium point, we plotted the initial N variation rate—which is approximately constant over the first 100 ps—as a function of μ, to obtain μ_{eq} from the zero intercept (Figure 4(b)). In this way we can estimate with a high precision the chemical potential (and hence the pressure) for the liquid-vapor coexistence of the model. Under the ideal gas approximation, this value of μ_{eq} implies a saturation pressure $P_0 = 0.486$ mbar at 298 K, which turns out to be two orders of magnitude below the corresponding experimental value, of 31.6 mbar. Such a discrepancy stems from the absence of rotational degrees of freedom in the mW model, which produces an entropy decrease that must be more significant in the gas phase than in the liquid, where rotations are restrained. As a consequence, in coarse-grained water there is a reduction of the free energy gap between the condensed and gas phases, that becomes manifest in a vapor pressure downshift. This difference between the experimental value of P_0 and the simulation result can be predicted in terms of the various contributions to the free energy in real water (μ^{exp}) and in the model (μ^{mW}):

$$\mu_L^{exp} = H_L^{exp} - T S_L^{exp} = H_L^{exp} - T\left(S_{id-tr}^{exp} + S_{id-rot}^{exp} + S_{xs}^{exp}\right), \quad (2)$$

$$\mu_L^{mW} = H_L^{mW} - T S_L^{mW} = H_L^{mW} - T\left(S_{id-tr}^{mW} + S_{xs}^{mW}\right), \quad (3)$$

where H_L and S_L are the molar enthalpy and entropy of the liquid phase, and the supraindex exp stands for experimental. The subindices $id-tr$ and $id-rot$ denote, respectively, the ideal gas contributions to translations and rotations, whereas xs refers to the excess entropy of the liquid with respect to the gas arising from the intermolecular interactions in the condensed phase. At the point of liquid-vapor coexistence, the chemical potentials of both phases must be equal:

$$\mu^{exp} = \mu_{exp}^{\theta} + RT \ln\left(\frac{P_{exp}}{P^{\theta}}\right) = H_L^{exp} - T\left(S_{id-tr}^{exp} + S_{id-rot}^{exp} + S_{xs}^{exp}\right), \quad (4)$$

$$\mu^{mW} = \mu_{mW}^{\theta} + RT \ln\left(\frac{P_{mW}}{P^{\theta}}\right) = H_L^{mW} - T(S_{id-tr}^{mW} + S_{xs}^{mW}), \quad (5)$$

The combination of these two last equations yields

$$\Delta\mu^{\theta} + RT \ln\left(\frac{P_{exp}}{P_{mW}}\right) = H_L^{exp} - H_L^{mW} - T S_{id-rot}^{exp} - T\left(S_{xs}^{exp} - S_{xs}^{mW}\right), \quad (6)$$

but, since $\Delta\mu^{\theta}$ is simply $-T S_{id-rot}^{exp}$, the equation above reduces to

$$RT \ln\left(\frac{P_{exp}}{P_{mW}}\right) = H_L^{exp} - H_L^{mW} - T\left(S_{xs}^{exp} - S_{xs}^{mW}\right) = \mu_{xs}^{exp} - \mu_{xs}^{mW}. \quad (7)$$

Adopting for μ_{xs}^{exp} and μ_{xs}^{mW}, respectively, values of −6.33 kcal/mol—from Ref. 54—and −8.63 kcal/mol—from our own Widom insertion simulations—, the predicted vapor pressure for the mW water model is $P_0 = P_{exp}\exp(\Delta\mu_{xs}/RT) = 0.68$ mbar, remarkably close to the value of 0.49 mbar estimated through our GCMD screening technique (it must be noticed that the deviation from 0.49 to 0.68 mbar originates in a difference of only 0.15 kcal/mol between the two values of $\Delta\mu_{xs}$).

The value of $\Delta\mu_{xs}$ can be broken down into its components, separating the enthalpic and the different entropic

contributions. On one hand, for the enthalpy we have $H_L^{exp} - H_L^{mW} = 0.09$ kcal/mol.[54] On the other hand, the two-body contribution to the translational part of the excess entropies, S_{2-tras}^{exp} and S_{2-tras}^{mW}, can be computed on the basis of the radial distribution functions obtained from neutron diffraction data[55] and from molecular dynamics simulations,[43] respectively, giving $T(S_{2-tras}^{exp} - S_{2-tras}^{mW}) = -0.10$ kcal/mol (where $S_{2-tras}^{exp} = -2.96$ cal/mol K and $S_{2-tras}^{mW} = -2.64$ cal/mol K). Therefore, the major contribution to the vapor pressure shift must come from the excess rotational entropy. This is formally equivalent to say that the entropy gain during the liquid-vapor transition is smaller for the monoatomic water model in comparison to real water, producing a decrease in its vapor pressure. Then, by tracking the origin of the decrease in P_0, we have demonstrated that the logarithm of the vapor pressure of the model is shifted with respect to the experimental value by a quantity equal to $(\mu_{xs}^{exp} - \mu_{xs}^{mW})/RT$.

Resorting to Gibbs ensemble Monte Carlo simulations with the Towhee code, we obtained an independent estimate of 0.458 mbar for the mW vapor pressure at 298 K. The small discrepancy with respect to our result of 0.486 mbar falls within the errors of the methodologies (see Sec. III C). Moreover, the average value of the particle density in the vapor phase turned out to be 1.1160×10^{-5} nm^{-3}, representing a deviation of less than 1% with respect to the ideal pressure, thus justifying the use of the ideal gas approximation.

Our method can be used to show that the mW model follows tightly the Clapeyron-Clausius equation, with a vaporization enthalpy of 10.60 kcal/mol. This result is in accurate agreement with the experimental value (10.52 kcal/mol at 298 K) and with the one reported in the original paper where the mW model was introduced (10.65 kcal/mol), in which ΔH_{vap} was obtained through canonical molecular dynamics simulations.[43] Figure 5 depicts the variation of $\ln P_0$ as a function of $1/T$ in the range 278–400 K. Each point in the graph was computed from a set of GCMD simulations at the corresponding temperature.

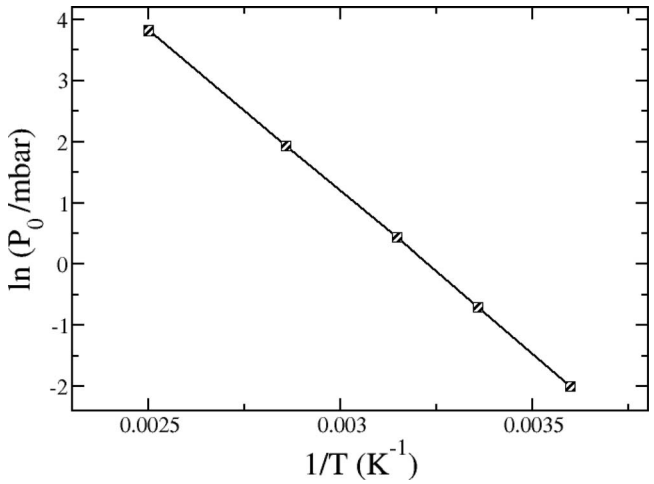

FIG. 5. Logarithm of the vapor pressure (in mbar) versus the inverse of the temperature for mW water. The model follows the Clapeyron-Clausius equation, with a vaporization enthalpy of 10.60 kcal/mol.

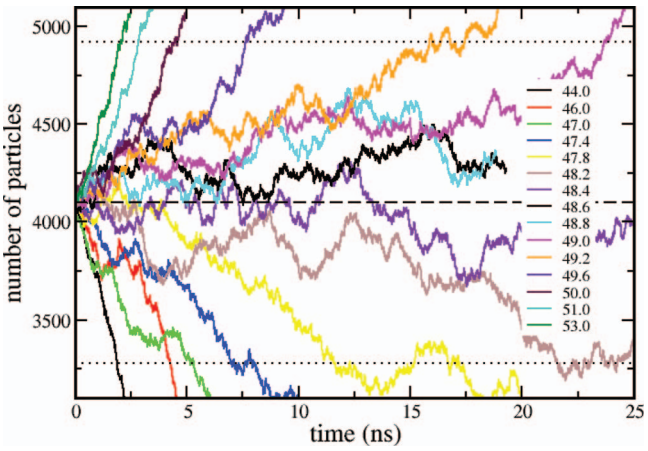

FIG. 6. Number of particles N as a function of time, in GCMD simulations of a slab of mW water for different pressures near the equilibrium value. The horizontal dashed line indicates the initial N (equal to 4102), whereas the dotted lines delimit a range of ±20% around this value. The legends indicate the pressure corresponding to each curve in units of mbar×100.

C. Precision in the determination of the equilibrium point

In principle, the present approach allows to reduce the error as much as desired, by performing a large enough number of simulations at different chemical potentials. In this section, this matter is examined in practice. What we find is that, in fact, the precision in the determination of μ_{eq} can be increased by further exploration of chemical potentials around the unknown equilibrium value. However, as μ approaches μ_{eq}, the ratio between effective particle insertions and deletions tends to 1, and therefore the sampling needs to be extended over longer times to reveal the final bias to evaporation or to condensation. Figure 6 exemplifies this behavior, by showing the number of molecules as a function of time in GCMD simulations of a water slab made of 4102 mW particles in a box of $7 \times 7 \times 10$ nm^3, for different pressures falling within $P_v \pm 10\%$. It can be seen that as μ is closer to the equilibrium value, insertions and deletions become more balanced, and the number of particles N fluctuates around the initial value for longer times. Such fluctuations are typically of the order of 10%. To decide whether evaporation or condensation has occurred, we can choose a threshold in terms of the (positive or negative) variation of N with respect to its initial value, which makes it possible to establish a connection between simulation times and the uncertainty in the estimation of P_v. To this end we adopt a variation of 20% (this makes a robust criterion as the trend predicted on its basis is never reverted if longer times are considered). The application of this criterion leads to Figure 7, which depicts the dependence of the error on the length of the simulation. Runs of 5 ns entail uncertainties of 3%, comparable with those informed in Gibbs ensemble grand canonical studies.[13,49,53] This error can be reduced by longer simulations. Nevertheless, Figure 7 suggests that it would be extremely expensive to go beyond an uncertainty of 1%, and therefore this limit can be taken as a nominal precision of the method for this particular system. Of course, the error will depend on both the model system and the temperature. Table I presents a similar analysis for the slab model

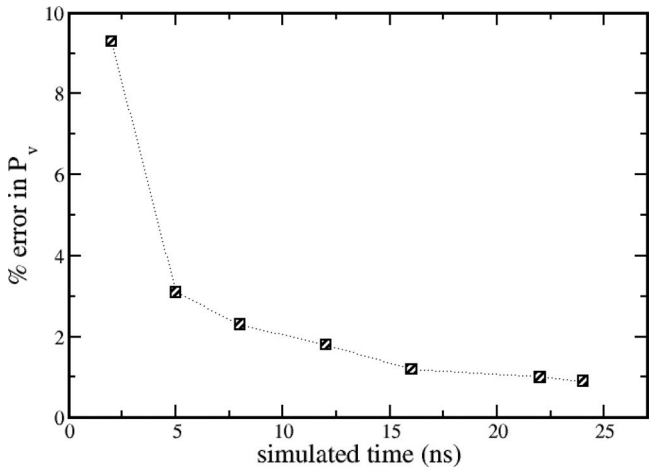

FIG. 7. Uncertainty in the determination of the vapor pressure of the mW model at 298 K, as a function of the sampled time in GCMD simulations. The data were obtained from the curves in Figure 6.

of argon studied in Sec. III A at two different temperatures, the highest of them in the vicinity of the critical point. Data from Gibbs ensemble simulations taken from Ref. 13 are also included. The errors exhibited in the table were obtained with sampling times of 3 ns. In these conditions the precision of the GCS approach is higher than that achieved with the Gibbs ensemble method, but lower than that corresponding to TMMC, which has been reported to be below 0.2%.[25]

As the temperature gets closer to the critical point, fluctuations in N become more significant. In the simulations at 150 K, we observed that a region exists where the trajectories may cross, violating the expected behavior, i.e., we see evaporation for a chemical potential μ_1 which is larger than a chemical potential μ_2 leading to condensation. This produces absolute errors in P_v of about two orders of magnitude higher than at 85 K. However, since the vapor pressure in turn increases exponentially, the relative errors end up differing by a factor of ten. The same trend for the relative errors is found in the Gibbs ensemble data (see Table I).

Fluctuations are discussed in a recent communication by Jackson and co-workers,[56] who demonstrate that these provide a significant contribution to the surface tension (through the free-energy variations) of small Lennard-Jones droplets. In particular, they argue that the mechanical route based on the pressure-tensor is not valid to compute the interfacial tension of nanodroplets because it does not capture the second-order energy fluctuations contribution. Here we would like to recall that fluctuations are significantly less important in water clusters than in the Lennard-Jones fluid, and, on the other hand, they are naturally considered in our approach, regardless of the magnitude of their contribution. On these grounds, we expect this technique to be equally valid for curved as much as for planar interfaces.

D. The vapor pressure of a water nanodroplet

We applied the GCS procedure to determine the vapor pressure of a water cluster of 94 molecules, using both the SPC/E and the mW potentials at 300 K. The sizes of the boxes were $5 \times 5 \times 5$ nm^3 and $4.9 \times 4.9 \times 8.6$ nm^3 for the SPC/E and mW calculations, respectively. At variance with simulations of argon droplets,[30] we found that the behavior of this system is not sensitive to the size of the simulation cell, unless it is extremely large. In that case, the probability that additional clusters nucleate in the given volume may not be negligible, leading to the appearance of multiple droplets coexisting in the gas phase.

The average radius of the droplet can be computed by identifying the position of the equimolar surface, R_e. If ρ_l and ρ_g are the bulk densities in the liquid and the vapor phase, this surface is defined by the following expression (see, for example, Ref. 31):

$$R_e^3 = \frac{1}{\rho_g - \rho_l} \int_0^\infty r^3 \frac{d\rho(r)}{dr} dr. \tag{8}$$

This integral is evaluated numerically on the radial density profiles. For the 94 molecules cluster, it gives a radius of 8.69 Å, which coincides with the one that can be deduced by simple inspection of the radial density profile.

In Figure 8, the number of water molecules is illustrated as a function of simulation step for a range of pressures. If the equilibrium pressures for SPC/E and mW are divided by the value of P_0 corresponding to each model, the relative vapor pressures resulting from both force-fields are in excellent agreement: 3.1 ± 0.1 and 2.9 ± 0.1 for SPC/E and mW respectively. The accord between both water models reflects that the P_0 shift observed in mW does not affect the ratio P/P_0 in the curved interface of the aggregate.

The Kelvin equation provides the vapor pressure (P_v) of a droplet as a function of the radius of curvature r of the interface:

$$\ln \frac{P_v}{P_0} = \frac{2\sigma}{r\rho RT}, \tag{9}$$

where P_0 is the vapor pressure of the bulk substance, σ is the surface tension, ρ is the density of the condensed phase, R is the gas constant, and T is the temperature. For very small droplets, of just a few nanometers of diameter, the effect of curvature on surface tension starts to be important. This can

TABLE I. Equilibrium chemical potentials (μ_{eq}, in kcal/mol) and vapor pressures (P_v, in bar) with the corresponding errors, calculated for the Lennard-Jones fluid.

This work					Gibbs ensemble Monte Carlo[13]		
T (K)	μ_{eq}	% error	P_v	% error	T (K)	P_v	% error
85	-2.2540 ± 0.0006	0.03	0.6781 ± 0.0025	0.37	90	0.9637 ± 0.1257	13
150	-3.2679 ± 0.0074	0.23	40.56 ± 1.01	2.5	150	42.32 ± 3.77	8.9

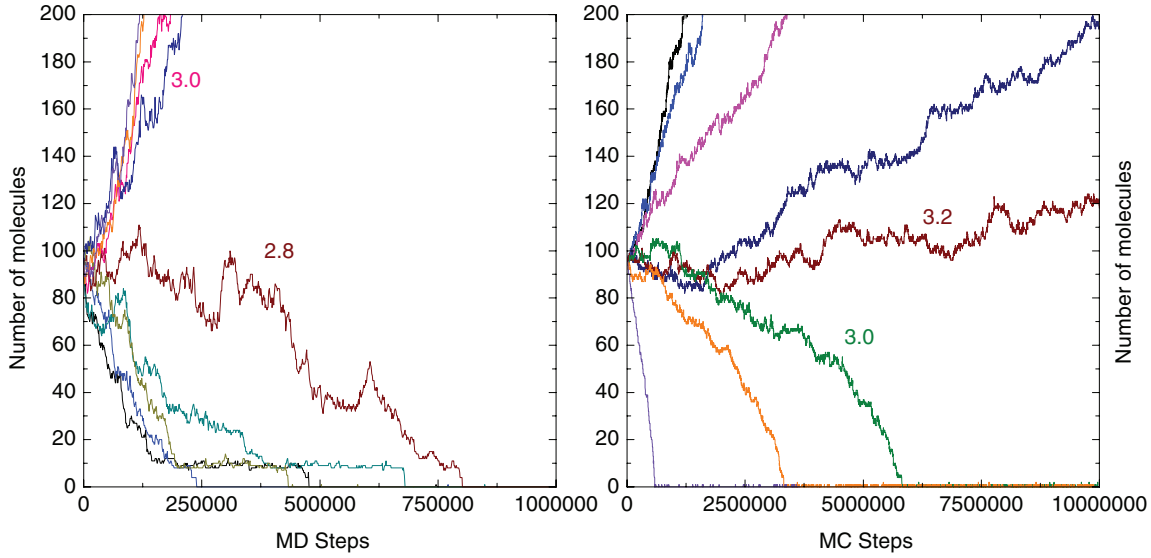

FIG. 8. Number of water molecules as a function of simulation step for a water droplet of 94 molecules, according to the mW (left) and the SPC/E (right) models at different pressures. Considering the equilibrium bulk vapor pressure of every model, mW and SPC/E yield, respectively, a ratio P/P_0 of 2.9 ± 0.1 and 3.1 ± 0.1 for this cluster. The relative pressures above and below the equilibrium value are labelled next to the curves.

be accounted for through the Tolman equation:[57]

$$\frac{\sigma}{\sigma_0} = \frac{1}{1 + 2\delta/r} \tag{10}$$

with σ_0 the surface tension of the planar interface, and δ the so-called Tolman length,[58] which assumes a characteristic value for every fluid. The combination of Eqs. (1) and (2) can in principle yield the dependence on radius of the vapor pressure. For water, the value of δ originally proposed by Tolman was 1 Å,[58] with more recent estimations falling always close to this former appraisal.[59,60] Adopting such a value to compute the surface tension of the interface for the cluster of 94 molecules, and setting $r = 8.69$ Å, the Kelvin equation turns out to be in remarkable agreement with the vapor pressure computed from our simulations. The results are compared in Table II.

IV. FINAL REMARKS

In summary, we have proposed a straightforward procedure to compute the vapor pressure of fluids in flat and curved interfaces. In bulk phases this property can be accessed via Gibbs ensemble simulations, which are however not appropriate for nanodroplets or other interfaces of arbitrary shape. The present algorithm can be equally applied to bulk or finite size model systems exposing an interface to the vacuum. We employed our scheme to find the vapor pressure of the mW model of water, showing that the result is consistent with a statistical thermodynamics analysis, and that the model follows the Clapeyron-Clausius law. The precision of the method appears comparable to that of the Gibbs ensemble approach, though it can be increased at the expense of computational time. Finally, we determined the vapor pressure of a water nanodroplet of 1.74 nm diameter, showing that it is in excellent agreement with the value predicted by the Kelvin equation if a Tolman length of 1 Å is considered.

We envision that one of the most significant applications of the GCS scheme would be the examination of binary or ternary aggregates that play a central role in the genesis of atmospheric aerosols.[12] The knowledge of how the vapor pressure of small water clusters is affected by the presence of sulfuric acid, or different organic compounds, is of enormous relevance in the investigation of homogeneous nucleation in the atmosphere, yet it is not trivially accessible through experiments, neither by simulations. The scheme we propose in this article can be equally applied to interfaces with one or more components. In particular, the liquid-vapor equilibrium

TABLE II. Relative vapor pressure for a water nanodroplet of 94 molecules, computed with the SPC/E model, the mW model, the Kelvin equation, and the Kelvin equation with the Tolman correction.

SPC/E	mW	Kelvin eq.	Kelvin + Tolman eq.
3.1	2.9	3.34	2.95

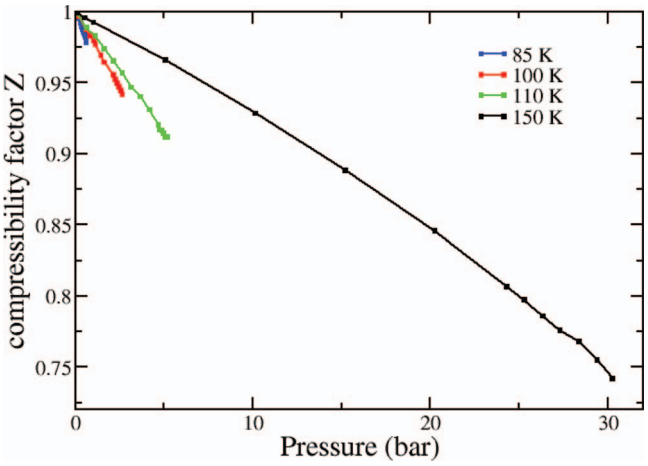

FIG. 9. Compressibility factors of the Lennard-Jones model as a function of pressure, obtained from isobaric-isothermal molecular dynamics simulations.

TABLE III. Vapor pressures (P_v) and corresponding fugacity coefficients (ϕ) computed for the Lennard-Jones model from integration of the compressibility factor.

Temperature (K)	P_v (mbar)	ϕ
85	0.6781	0.984
100	2.896	0.949
110	5.702	0.921
150	40.56	0.743

in binary clusters of water and sulfuric acid of different size and composition will be the subject of future investigations.

ACKNOWLEDGMENTS

We express our gratitude to Professor Ernesto Marceca and to Dr. Damian Bikiel for valuable discussions. This study has been supported by a collaborative grant of the Agencia Nacional de Promocion Cientifica y Tecnologica de Argentina, PICT 2007-2111 to V.M. and D.A.S. We acknowledge the Center of High Performance Computing of the University of Utah for technical support and allocation of computing time.

APPENDIX: FUGACITY COEFFICIENTS OF ARGON

The non-ideal vapor pressure P_v can be computed from the equilibrium chemical potential according to $\mu_{eq} = k_B T \ln \Lambda^3 + k_B T \ln(P_v \phi / k_B T)$, where Λ is the de Broglie length and ϕ is the fugacity coefficient at the corresponding pressure and temperature. These coefficients can be extracted from a set of molecular dynamics simulations at different pressures in the isobaric-isothermal ensemble. From such simulations it is possible to obtain the dependence of the compressibility factor ($Z = V_m / V_m^{ideal}$) on P. Once this dependence is known for a given temperature, $\phi(P)$ can be calculated by integration of $(Z-1)/P$ up to the desired pressure. In this work, NPT simulations were conducted on systems of 1000 particles at 85, 100, 110, and 150 K, over a range of pressures from zero to coexistence. Figure 9 shows the compressibility factor as a function of P for the different temperatures examined. On the other hand, Table III presents the fugacity coefficients determined for the argon model at the coexistence pressure.

[1] F. Rouquerol, J. Rouquerol, and K. Sing, *Adsorption by Powders and Porous Solids*, 1st ed. (Academic Press, 1999).
[2] R. Kematick and C. E. Myers, Chem. Mater. **8**, 287 (1996).
[3] M. Yoshizawa, W. Xu, and C. A. Angell, J. Am. Chem. Soc. **125**, 15411 (2003).
[4] M. C. R. S. Kodambaka, J. Tersoff, and F. M. Ross, Science **316**, 729 (2007).
[5] C. H. See and A. T. Harris, Ind. Eng. Chem. Res. **46**, 997 (2007).
[6] S. Choi, A. Jamshidi, T. J. Seok, M. C. Wu, T. I. Zohdi, and A. P. Pisano, Langmuir **28**, 3102 (2012).
[7] P. Peeters, J. Hrubý, and M. E. H. van Dongen, J. Phys. Chem. B **105**, 11763 (2001).
[8] A. Shavorskiy, F. Aksoy, M. E. Grass, Z. Liu, H. Bluhm, and G. Held, J. Am. Chem. Soc. **133**, 6659 (2011).
[9] M. Mandal and K. Landskron, Acc. Chem. Res. **46**, 2536 (2013).
[10] W. H. Rodebush, Proc. Natl. Acad. Sci. U.S.A. **40**, 789 (1954).
[11] M. O. Andreae, Science **339**, 911 (2013).
[12] R. Zhang, A. Khalizov, L. Wang, M. Hu, and W. Xu, Chem. Rev. **112**, 1957 (2012).
[13] A. Panagiotopoulos, N. Quirke, M. Stapleton, and D. Tildesley, Mol. Phys. **63**, 527 (1988).
[14] A. Panagiotopoulos, J. Phys. Condens. Matter **12**, R25 (2000).
[15] D. Frenkel and B. Smit, *Understanding Molecular Simulation*, 2nd ed. (Academic Press, 2002)
[16] A. Lyubartsev, A. Martsinovski, S. Shevkunov, and P. Vorontsov-Velyaminov, J. Chem. Phys. **96**, 1776 (1992).
[17] E. Marinari and G. Parisi, Europhys. Lett. **19**, 451 (1992).
[18] M. Mezei, J. Comput. Phys. **68**, 237 (1987).
[19] A. Bruce and N. Wilding, Adv. Chem. Phys. **127**, 1 (2003).
[20] G. R. Smith and A. D. Bruce, J. Phys. A: Math. Gen. **28**, 6623 (1995).
[21] M. Fitzgerald, R. R. Picard, and R. N. Silver, Europhys. Lett. **46**, 282 (1999).
[22] J.-S. Wang, T. K. Tay, and R. H. Swendsen, Phys. Rev. Lett. **82**, 476 (1999).
[23] J.-S. Wang, Comput. Phys. Commun. **121–122**, 22 (1999).
[24] J.-S. Wang and R. H. Swendsen, J. Stat. Phys. **106**, 245 (2002).
[25] J. K. Errington, J. Chem. Phys. **118**, 9915 (2003).
[26] A. S. Paluch, V. K. Shen, and J. R. Errington, Ind. Eng. Chem. Res. **47**, 4533 (2008).
[27] K. S. Rane, S. Murali, and J. R. Errington, J. Chem. Theory Comput. **9**, 2552 (2013).
[28] V. Kumar and J. R. Errington, J. Chem. Phys. **138**, 174112 (2013).
[29] E. M. Grzelak and J. R. Errington, J. Chem. Phys. **132**, 224702 (2010).
[30] S. Fujikawa, T. Yano, and M. Watanabe, *Vapor Liquid Interfaces, Bubbles and Droplets. Fundamentals and Applications* (Springer-Verlag, Berlin/Heidelberg, 2011).
[31] S. M. Thompson and K. E. Gubbins, J. Chem. Phys. **81**, 530 (1984).
[32] A. P. Shreve, J. P. R. B. Walton, and K. E. Gubbins, J. Chem. Phys. **85**, 2178 (1986).
[33] M. J. P. Nijmeijer, C. Bruin, A. B. van Woerkom, A. F. Bakker, and J. M. J. van Leeuwen, J. Chem. Phys. **96**, 565 (1992).
[34] M. P. Moody and P. Attard, Phys. Rev. Lett. **91**, 056104 (2003).
[35] S. Plimpton, J. Comput. Phys. **117**, 1 (1995).
[36] M. G. Martin, B. Chen, C. D. Wick, J. J. Potoff, J. M. Stubbs, and J. I. Siepmann, MCCCS Towhee, Version 7.0.6, see http://towhee.sourceforge.net (2013).
[37] H. J. Berendsen, J. R. Grigera, and T. P. Straatsma, J. Phys. Chem. **91**, 6269 (1987).
[38] A. Papadopoulou, E. D. Becker, M. Lupkowski, and F. van Swol, J. Chem. Phys. **98**, 4897 (1993).
[39] G. S. Heffelfinger and F. van Swol, J. Chem. Phys. **100**, 7548 (1994).
[40] G. Arya, H.-S. Chang, and E. J. Maginn, J. Chem. Phys. **115**, 8112 (2001).
[41] R. F. Cracknell, D. Nicholson, and N. Quirke, Phys. Rev. Lett. **74**, 2463 (1995).
[42] J. O. Hirschfelder, C. F. Curtiss, and R. B. Bird, *Molecular Theory of Gases and Liquids*, 2nd ed. (John Wiley and Sons, 1964).
[43] V. Molinero and E. B. Moore, J. Phys. Chem. B **113**, 4008 (2009).
[44] E. B. Moore and V. Molinero, Nature (London) **479**, 506 (2011).
[45] J. Puibasset and R. J.-M. Pellenq, J. Chem. Phys. **118**, 5613 (2003).
[46] J. Puibasset and R. J.-M. Pellenq, J. Phys. Chem. B **112**, 6390 (2008).
[47] A. Malani and K. G. Ayappa, J. Phys. Chem. B **113**, 1058 (2009).
[48] E. Tombácz, A. Hajdú, E. Illés, K. László, G. Garberoglio, and P. Jedlovszky, Langmuir **25**, 13007 (2009).
[49] J.-C. Liu and P. A. Monson, Langmuir **21**, 10219 (2005).
[50] J. R. Errington and A. Z. Panagiotopoulos, J. Phys. Chem. B **102**, 7470 (1998).
[51] C. Vega and E. de Miguel, J. Chem. Phys. **126**, 154707 (2007).
[52] C. Vega and J. L. F. Abascal, Phys. Chem. Chem. Phys. **13**, 19663 (2011).
[53] A. K. Al-Matar, A. H. Tobgy, and I. A. Suleiman, Mol. Simul. **34**, 289 (2008).
[54] W. Wagner and A. Pruß, J. Phys. Chem. Ref. Data **31**, 387 (2002).
[55] L. B. Skinner, C. Huang, D. Schlesinger, L. G. M. Pettersson, A. Nilsson, and C. J. Benmore, J. Chem. Phys. **138**, 074506 (2013).
[56] J. G. Sampayo, A. Malijevský, E. A. Muller, E. de Miguel, and G. Jackson, J. Chem. Phys. **132**, 141101 (2010).
[57] R. C. Tolman, J. Chem. Phys. **17**, 333 (1949).
[58] R. C. Tolman, J. Chem. Phys. **17**, 118 (1949).
[59] H. M. Lu and Q. Jiang, Langmuir **21**, 779 (2005).
[60] Y.-Q. Xue, X.-C. Yang, Z.-X. Cui, and W.-P. Lai, J. Phys. Chem. B **115**, 109 (2011).
[61] *NIST Chemistry WebBook*, NIST Standard Reference Database Number 69, fitting by L. I. Drii and V. A. Rabinovich (National Institute of Standards and Technology, 2011); see http://webbook.nist.gov.